Mineral Spectroscopy: A Tribute to Roger G. Burns
© The Geochemical Society, Special Publication No. 5, 1996
Editors: M. D. Dyar, C. McCammon and M. W. Schaefer

An occurrence of jarositic tephra on Mauna Kea, Hawaii: Implications for the ferric mineralogy of the Martian surface

RICHARD V. MORRIS,[1] DOUGLAS W. MING,[1] D. C. GOLDEN[2] and JAMES F. BELL, III[3]

[1]NASA Johnson Space Center, Houston, TX 77058, U.S.A.
[2]Dual Inc., Houston, TX 77058, U.S.A.
[3]Center for Radiophysics and Space Research, Cornell University, Ithaca, NY 14853, U.S.A.

Abstract—A sample of yellow-colored tephra (HWMK24) from a cone on the summit of Mauna Kea, Hawaii, was examined by a variety of analytical techniques, including X-ray diffraction, scanning electron microscopy, Mössbauer spectroscopy, and visible and near-IR reflectance spectroscopy. The yellow pigment was determined to be the ferric hydroxysulfate jarosite ($(H_3O,Na,K)Fe_3\times(SO_4)_2(OH)_6$) by positions of the (101), (003), (021), (033), and (220) reflections in the XRD powder pattern, 0.35 mm/s isomer shift and 1.19 mm/s quadrupole splitting for the Mössbauer doublet, and well-defined band minima at 430, 910, 1480, and 1840 nm in reflectivity spectra. The XRD, Mössbauer, and reflectivity data also indicate that phyllosilicates are not present and that jarosite is the predominant iron-bearing phase. As determined by SEM imaging, the jarosite has a cubic morphology and occurs as aggregates of individual crystals on exterior surfaces and in vesicles. Jarosite formation in HWMK24 likely proceeded by hydrothermal dissolution of silicate glass and minerals by sulfuric acid solutions (from volcanic SO_2 and H_2O gases) and subsequent precipitation, under oxidizing conditions, of relatively insoluble jarosite (K-rich) during or shortly after cone formation. The occurrence of band minima near 910 nm in spectral data for certain Martian regions (*e.g.*, East and West Oxia and Lunae Planum) might indicate the presence of jarosite formed during acid-sulfate weathering, possibly in conjunction with SO_2 gases release during Martian volcanism.

INTRODUCTION AND BACKGROUND

THE MINERALOGY of iron-bearing weathering products on the Martian surface is largely constrained by the Viking Lander geochemical and magnetic properties experiments and by earth-based telescopic and spacecraft spectral observations at visible and near-IR wavelengths. Elemental abundances provided by the Viking X-ray fluorescence experiment (CLARK *et al.*, 1982) constrain mineralogy to the extent that mineral assemblages must be consistent with bulk composition. The magnetic properties experiment implies that a 1–7 wt. % strongly magnetic component is present in Martian fines (HARGRAVES *et al.*, 1977, 1979). Mineralogies that have been suggested for this component include Fe-Ti spinels (magnetites and maghemites), pyrrhotite, feroxyhyte, and nanophase hematite (HARGRAVES *et al.*, 1979; BURNS, 1980, 1988; MOSKOWITZ and HARGRAVES, 1982; POSEY-DOWTY *et al.*, 1986; MORRIS *et al.*, 1989, 1990; COEY *et al.*, 1990). All these mineralogies are consistent with the elemental data for 1–7 wt. % magnetic component. Earth-based telescopic data of Martian bright regions (weathered Martian surface material) are characterized by an absorption edge extending from approximately 400 to 750 nm with inflections near 520 and 600 nm, a relative reflectivity maximum near 750 nm, and a shallow absorption band centered near 860 nm (*e.g.*, SINGER *et al.*, 1979; MCCORD *et al.*, 1982; SINGER, 1985; BELL *et al.*, 1990). Spectral data from the Phobos-2 spacecraft, which have significantly better spatial resolution than the telescopic data, confirm the presence of surface regions with a ~860 nm band minimum and also show other regions where the shallow band minimum is located as high as ~910 nm (MURCHIE *et al.*, 1993). It is not known whether the other spectral features indicated above also change position because the Phobos-2 data do not extend to wavelengths shorter than ~800 nm. Composite spectra for Martian bright regions with the 860 nm band have been published by SINGER *et al.* (1979) and MUSTARD and BELL (1994). What mineralogies are implied by the positions of these spectral features?

Analyses of both synthetic and naturally-occurring spectral analogues of Mars have been important for making specific mineralogical assignments for Martian spectral features. For synthetic samples, MORRIS *et al.* (1989) and MORRIS and LAUER (1990) showed that nanophase hematite particles (hematite particles having diameters less than ~10 nm) and subordinate amounts of well-crystalline hematite dispersed in spectrally-neutral matrix materials can reproduce spectral data for Martian bright regions where the shallow ~860 nm band is present. The ferric absorption edge results predominantly from absorption by nanophase he-

matite and the shallow 860 nm band, 750 nm relative reflectivity maximum, and 600 and 520 nm inflections are all features traceable to well-crystalline hematite. Identification of well-crystalline hematite on Mars is unequivocal to the extent that hematite spectral features are unique. Nanophase hematite, however, does not have diagnostic spectral features, so its presence is consistent with (but not required by) Martian spectral data. Other nanophase ferric oxides may be present instead.

For naturally-occurring material, samples that contain palagonite (weathering product of mafic volcanic glass) have received considerable attention, in part because palagonitic samples are generally reasonable Martian spectral analogues (EVANS and ADAMS, 1979, 1980; BERKLEY and DRAKE, 1981; ALLEN *et al.* 1981; SINGER, 1982; MORRIS *et al.*, 1990, 1993; BELL *et al.*, 1993; GOLDEN *et al.*, 1993) and in part because processes favorable to palagonite formation are considered to be active on Mars, both now and in times past. These processes include hydrothermal alteration induced by hot, oxidizing fluids and/or gases mobilized by impact events, volcanism, or geothermal gradients (NEWSOM, 1980; ALLEN *et al.*, 1982; BELL *et al.*, 1993; MORRIS *et al.*, 1995), subpermafrost magmatic intrusion (SODERBLOM and WENNER, 1978; ALLEN *et al.*, 1981), subaerial extrusion above the permafrost layer (BERKLEY and DRAKE, 1981), and static gas-glass weathering (GOODING and KEIL, 1978). Samples of palagonitic tephra collected from the same location on the Puu Nene cinder cone on Mauna Kea Volcano, Hawaii, are among the best spectral analogues and have been studied in detail as sample Hawaii-34 (EVANS and ADAMS, 1979, 1980), VOLO2A (SINGER, 1982), and PN-9 (MORRIS *et al.*, 1993).

EVANS and ADAMS (1979, 1980) reported spectral data for Hawaii-34 and showed that its nearly constant reflectivity in the near-IR and strong absorption edge through the visible were very similar to Martian bright regions spectra. Based on compositional data and the absence of coherent scattering in powder X-ray diffraction patterns, they concluded that the palagonitic tephra was primarily iron allophane (an iron-rich amorphous hydrated aluminosilicate gel) with iron present as Fe^{3+}. The absence of well-defined Fe^{3+} crystal-field bands was attributed to the lack of long-range crystalline ordering as observed in the XRD data. SINGER (1982), who obtained similar spectral, compositional, and XRD data for sample VOLO2A, also argued that the low intensity of Fe^{3+} crystal-field bands apparently results from the lack of crystalline order. Although not explicitly stated, the discussion of the XRD data in these studies implies a model where iron is present as isolated paramagnetic Fe^{3+} ions at sites having highly-variable size and distortion. In addition to reproducing the spectral and XRD data for Hawaii-34 and VOLO2A for sample PN-9, MORRIS *et al.* (1993) reported observations made with transmission electron microscopy and data from spectral and Mössbauer measurements of size and magnetic separates which were subjected to chemical extraction procedures to determine the siting of Fe^{3+}. These data showed that the Fe^{3+} is present as discrete particles having dimensions less than ~20 nm (*i.e.*, nanophase ferric oxide) embedded in a hydrated aluminosilicate matrix and that these particles are responsible for the strong ferric absorption edge. The nanophase ferric oxide particles were not detected in XRD data because they are too small to coherently scatter X-rays. The XRD mineralogy of these particles is uncertain, but electron diffraction indicates the mineralogy of these nanophase particles is nanophase hematite and/or ferrihydrite (MORRIS *et al.*, 1993).

The iron mineralogy of both synthetic and palagonitic samples provides a strong basis for inferring the presence of well-crystalline hematite for Martian bright regions which are characterized by spectral data with a ~860 nm band minimum. Other ferric mineralogies are implied for regions with band minima near 910 nm. As noted by MURCHIE *et al.* (1993), potential mineralogies include the ferric hydroxysulfate jarosite, which has the general composition $((H_3O,Na,K)Fe_3(SO_4)_2(OH)_6)$. Iron-bearing sulfates like jarosite are possible mineralogies because sulfur is a chemically important component of Martian surface materials (~7% SO_3 (CLARK *et al.*, 1982)) and because the phase will probably precipitate under Martian surface conditions (BURNS, 1988, 1993; BURNS and FISHER, 1990a,b). Are jarosites reasonable assignments when all spectral features are considered; for example, are the jarosite 1480 and 1840 nm bands present? Are there spectral analogues among altered tephra samples from Mauna Kea that contain sulfates and have shallow band minima near 910 nm? The only ferric-bearing alteration products observed to date are nanophase ferric oxide, hematite, and titanohematite (*e.g.*, BELL *et al.*, 1993; GOLDEN *et al.*, 1993; MORRIS *et al.*, 1993).

In this paper, we report an occurrence of oxidatively-altered tephra (sample HWMK24) from the summit of Mauna Kea in which the dominant ferric mineralogy is jarosite. The implication of its spectral data and formation conditions are discussed with respect to the potential occurrence of the phase on Mars. In addition to spectral data, the

jarosite-bearing tephra was characterized by powder X-ray diffraction analysis, Mössbauer spectroscopy, and photomicrographs obtained by scanning electron microscopy. For purposes of comparison, corresponding data were also obtained for four other terrestrial occurrences of jarosite.

SAMPLES AND METHODS

Samples

HWMK24. Sample is yellow-colored tephra collected from a road cut on the northwest flanks of the unnamed summit cone of Mauna Kea Volcano upon which the Japan National Subaru Telescope is located. The cone is part of the Laupahoehoe Volcanics (hawaiitic composition) which form the magmatically evolved cap of Mauna Kea (WOLFE *et al.,* 1996). The tephra occurs as a layer ~50 cm wide and ~5 cm high. The sample was later fractionated in the laboratory by dry sieving with a 1 mm sieve. A <5 μm separate was obtained from part of the <1 mm fraction by ultrasonic dispersion and water sedimentation. Several tephra particles 1–4 cm in diameter were ground to fine powders (<90 μm).

LNVJAR1. Sample is a fine powder (<90 μm) of a hand sample of massive jarosite from Luning, NV (obtained from Wards Natural Science Establishment).

GCJAR1. Sample is a fine powder (<90 μm) of a hand sample of jarositic material from Grant County, NM. Location and description of the sample has been documented by NORTHROP and WHITNEY (1987).

TT#12 and TT#35. Samples are <1 mm sieve fractions of jarositic soil that have been previously examined by TOWNSEND (1987). They are his samples 12F and 35F and were collected near Goldfield, NV.

Methods

A Cary-14 spectrophotometer configured with a 14 cm diameter integrating sphere was used to obtain visible and near-IR reflectance spectra. Ranger Mössbauer spectrometers using ^{57}Co(Rh) sources were used to obtain iron Mössbauer spectra. Mössbauer spectra were fit to theoretical line shapes by an in-house computer program. A Scintag XDS 2000 X-ray diffractometer using CuK radiation was employed to obtain powder X-ray diffraction patterns. A JEOL JSM-35CF scanning electron microscope equipped with a PGT EDS was employed for SEM imaging and chemical analysis. More detailed information on analytical procedures is given by MORRIS *et al.* (1989, 1990), GOLDEN *et al.* (1993), and BELL *et al.* (1993).

RESULTS AND DISCUSSION

X-ray diffraction

Throughout this paper, we will use the name jarosite to refer to the general composition $(H_3O,Na,K)Fe_3(SO_4)_2(OH)_6$, although the name actually refers to the K endmember. The H_3O and Na endmembers are hydronium jarosite and natrojarosite, respectively. Jarosite was identified in all

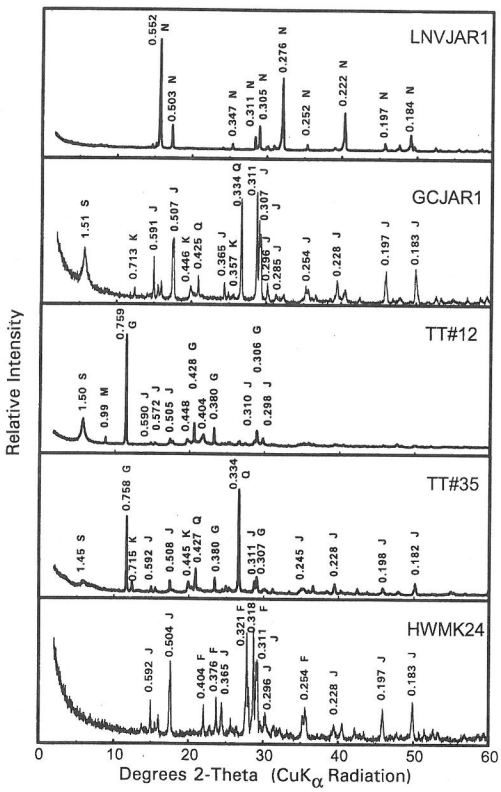

FIG. 1. X-ray diffraction patterns for jarosite-containing samples LNVJAR1 (Luning, NV), GCJAR1 (Grant Co., NM), TT#12 and TT#35 (Goldfield, NV), and HWMK24 (<1 mm; Mauna Kea, HW). All **d**-spacings are in nm. K = kaolinite, S = smectite, Q = quartz, G = gypsum, M = mica, J = jarosite, N = natrojarosite, F = plagioclase feldspar.

five samples (Fig. 1), although the apparent quantities in the samples varies significantly as suggested by XRD peak intensities. LNVJAR1 was monomineralic natrojarosite (Fig. 1). Primary peaks used to identify natrojarosite were 0.552 nm (003) and 0.276 nm (006) peaks. The high-intensity diffraction peaks for the (003) and (006) indicate a highly-oriented sample along the **c**-axis.

In addition to jarosite (K-rich as indicated by SEM EDS analysis), GCJAR1 contained smectite, quartz, and minor amounts of kaolinite. The primary XRD **d**-spacings used to identify (K-rich) jarosite were 0.592 nm (101), 0.572 nm (003), 0.311 nm (021), 0.197 nm (033), and 0.183 nm (220) peaks. The sharp, narrow diffraction peaks of jarosite in GCJAR1 indicate a high degree of crystallinity. TT#12 and TT#35 contained minor quantities of jarosite as indicated by weak diffraction peaks (Fig. 1). TT#12 sample contained pri-

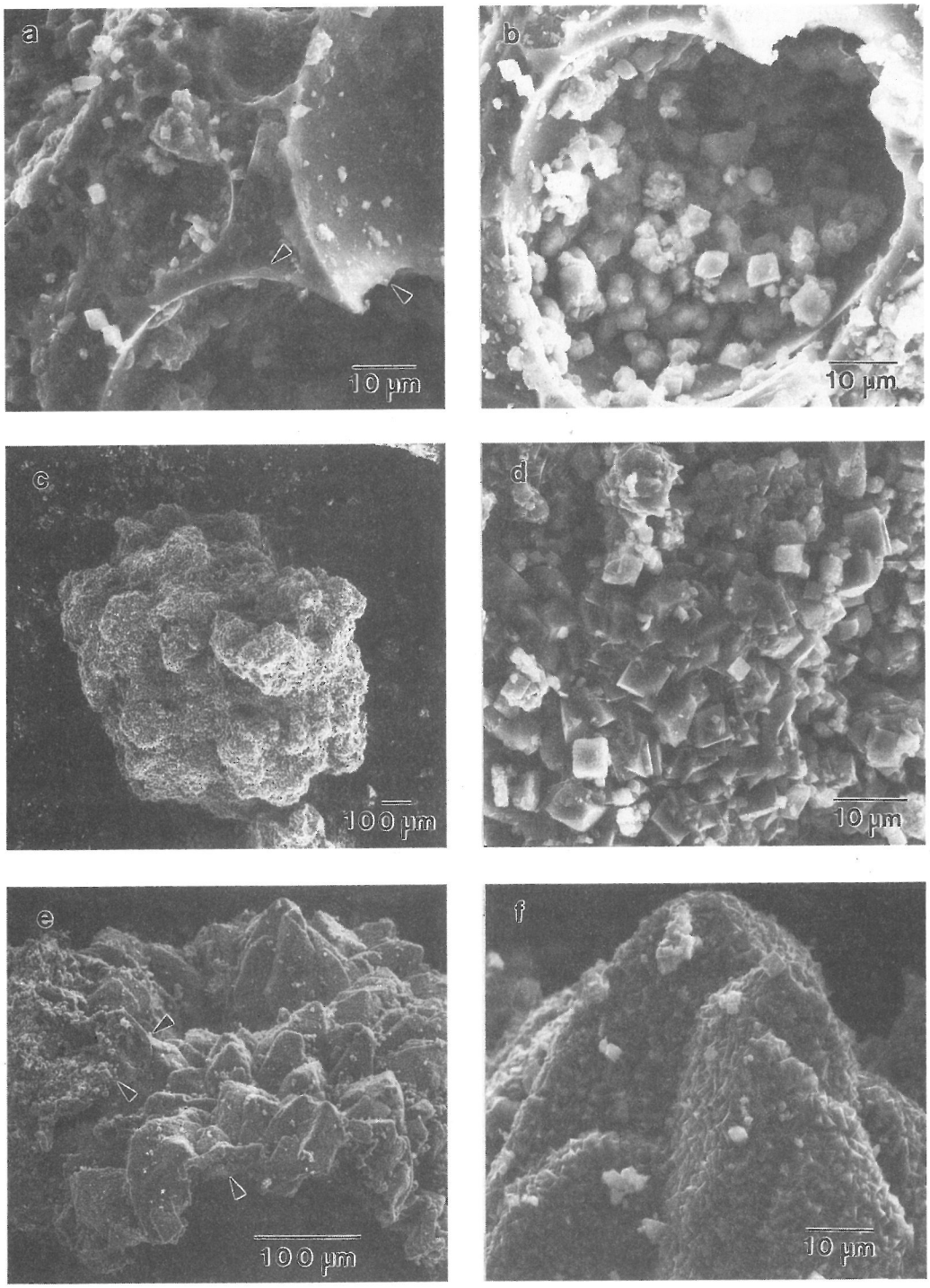

FIG. 2. Scanning electron micrographs of jarosite from the Mauna Kea tephra. (a) dissolution of intervesicular wall and dissolution pits in glass (arrows); (b) jarosite crystals precipitated in glass vesicles; (c) jarosite replica of an unknown cluster of cubic crystals; (d) jarosite cubes enlarged from (c); (e) jarosite replica of an unknown cluster of prismatic crystals (arrows show hollow interior of replica); (f) jarosite cubes enlarged from (e).

marily gypsum and lesser amounts of smectite and mica. Gypsum and quartz dominated the mineralogy of the TT#35. This sample also contained minor quantities of smectite and kaolinite. Stronger peak intensities for jarosite in TT#35 suggested more jarosite in this sample as compared to TT#12.

Jarosite (K-rich as indicated by SEM EDS analysis) and plagioclase feldspar (Ca-rich) were the major phases identified in the Mauna Kea tephra (sample HWMK24, <1 mm). No phyllosilicates were detected. The XRD pattern for jarosite in HWMK24 is very similar to the pattern obtained for jarosite in GCJAR1. The sharp, narrow diffraction peaks of jarosite in sample HWMK24 indicate a high degree of crystallinity, which is supported by SEM morphological analysis discussed next.

Scanning electron microscopy

Morphological characteristics of jarosite in the Mauna Kea tephra are photogenic and are nearly identical with those reported in soils (*e.g.,* DIXON *et al.,* 1982; DONER and LYNN, 1989). The jarosite from GCJAR1 has a similar morphology to the jarosite in the tephra. Scanning electron photomicrographs of jarosite from HWMK24 are shown in Fig. 2. The jarosite occurs ubiquitously as aggregates of individual cubic crystals that are 2–5 μm in size. The aggregates normally are present as small clusters on exterior surfaces or within glass vesicles (Fig. 2a,b). Two unrepresentative aggregates of jarosite crystals were noted (Fig. 2c-f). Thin layers of cubic jarosite crystals appear to have replicated the form of larger crystals. In Fig. 2e, the broken edge indicates the jarosite replication has separated from the larger crystals, and the overturned rind (arrows) shows the hollow interior of the replica.

The occurrence of jarosite crystals in glass vesicles (Fig. 2a,b) suggests precipitation from acid sulfate solutions. Acid sulfate weathering conditions which produce sulfuric acid have apparently facilitated dissolution of intervesicular walls (Fig. 2a) and formation of dissolution pits in glass and plagioclase feldspar (not shown). Energy dispersive spectroscopy showed that the jarosite is K-rich (data not shown).

Mössbauer spectroscopy

The Mössbauer spectra of all five samples are shown in Fig. 3, and the jarosite Mössbauer parameters are compiled in Table 1. The average values of IS and QS for the jarosite Fe^{3+} doublet, which are 0.35 ± 0.02 mm/s and 1.19 ± 0.02 mm/s at room temperature, are within the range published in the literature (STEVENS *et al.,* 1983). Jarosite is the only iron-bearing phases detected for GCJAR1, TT#12, and TT#35. For HWMK24, jarosite is virtually the only iron-bearing phase detected for the <5 μm and <1 mm size fractions. Minor amounts of other iron-bearing mineralogies (especially for the <1 mm fraction) are indicated by low-intensity sextets (probably hematite and (titano)magnetite) and low-intensity ferrous doublets (probably glass and olivine).

Mössbauer spectra of powders of 1–4 cm tephra particles from HWMK24 were highly variable. The spectrum of HWMK24-R3 (Fig. 3), which is a powder of a coherent, dense tephra particle, is dominated by ferrous mineralogies. Its spectrum is very similar to that published by MORRIS *et al.* (1993) for hawaiitic basalt HAW-16, for which the major iron-bearing phases are olivine and titanomagnetite. This type of material is probably the ferrous-bearing component in the spectrum of HWMK24 (<1 mm). Mössbauer spectra for powders of friable, vesicular (porous) tephra particles were inter-

Table 1. Phase identification based on XRD, values of Mössbauer parameters (IS and QS) for jarosite doublets, and positions of band minima for ferric $^6A_1 \rightarrow {}^4T_{1g}$ and $^6A_1 \rightarrow ({}^4E, {}^4A)$ electronic transitions. Phases are listed in order of apparent decreasing abundance based on XRD peak intensities.

Sample	Phases Based on XRD	IS (mm/s)	QS (mm/s)	$^4T_{1g}$ (nm)	$^4E, {}^4A$ (nm)
LNVJAR1	jarosite (natrojarosite)	0.36	1.19	920	434
GCJAR1	jarosite, smectite, quartz, kaolinite	0.33	1.20	920	432
TT#12	gypsum, smectite, mica, jarosite	0.33	1.22	910	432
TT#35	quartz, gypsum, jarosite, kaolinite, smectite	0.33	1.20	918	432
HWMK24	<1 mm: jarosite, plagioclase	0.38	1.19	910	432
HWMK24	<5 μm: jarosite	0.36	1.15	910	432
Uncertainty		0.01	0.01	8	5

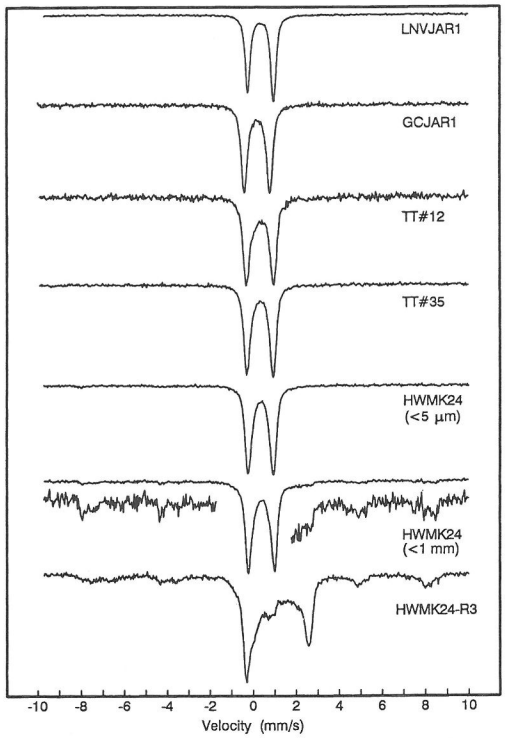

FIG. 3. Mössbauer spectra at 298 K. The spectra of LNVJAR1, GCJAR1, TT#12, TT#35, and HWMK24 (<1 mm and <5 μm) are characterized by a doublet resulting from Fe^{3+} in jarosite. The spectrum of HWMK24-R3, which is a powder of a dense, coherent 1–4 cm diameter tephra particle, is complex but contains a doublet resulting from Fe^{2+} in olivine and sextets resulting from Fe^{2+} and Fe^{3+} in (titano)magnetite.

mediate to those for HWMK24 (<1 mm) and HWMK24-R3. In keeping with SEM data, these results imply that the jarosite is formed by penetration of sulfur-bearing gases and/or fluids or gases through porous and glassy tephra under oxidizing conditions. Tephra particles like HWMK24-R3 are relatively impervious and are not altered to jarosite. This view is supported by observations made during pulverization of the large tephra particles. Coherent particles like HWMK24-R3 had a yellow (jarosite) rind or coating and black (hawaiitic) interiors, and friable particles were yellow with scattered black islands throughout their volume.

Diffuse reflectance spectroscopy

Reflectivity spectra are shown in Fig. 4; the spectrum of LNVJAR1 is equivalent to jarosite spectra published previously (*e.g.*, HUNT *et al.*, 1971; HUNT and ASHLEY, 1979; CLARK *et al.*, 1990). All spectral features at wavelengths shorter than 1100 nm result from ferric iron, which has four electronic transitions in this spectral region. Three are single-electron transitions from the $^6A_1$ ground state of ferric iron to the (^4E,^4A), $^4T_{2g}$, and $^4T_{1g}$ levels of its first (quartet) excited state and one is a pair transition of two electrons from two magnetically coupled ferric ions from $^6A_1$ to $^4T_{1g}$ (SHERMAN *et al.*, 1982; MORRIS *et al.*, 1985; SHERMAN and WAITE, 1985). The well-defined band minima near 430 and 920 nm are assigned to the (^4E,^4A) and $^4T_{1g}$ transitions, respectively. The region between the inflection near 600 nm and the relative reflectivity maximum near 720 nm is a manifestation of the unresolved $^4T_{2g}$ transition, and the region between the two inflections near 480 and 600 nm is a manifestation of the pair transition.

As shown best by the spectrum of LNVJAR1, jarosite also has two sharp bands near 1480 and

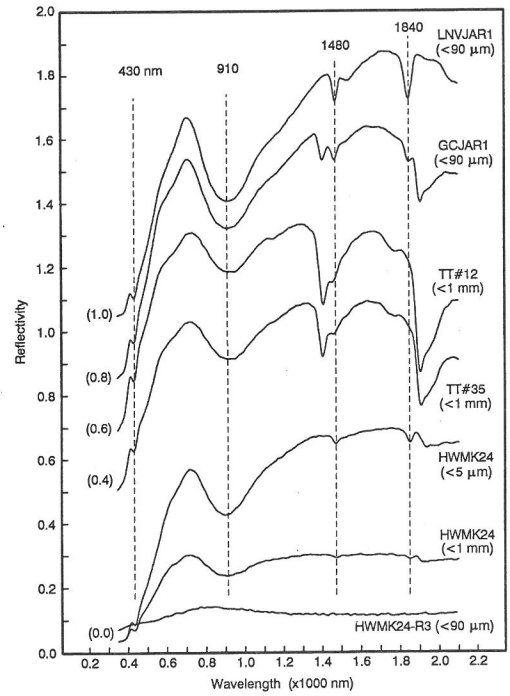

FIG. 4. Reflectivity spectra at 298 K. The spectra of LNVJAR1, GCJAR1, and HWMK24-R3 are for fine powders (<90 μm); TT#12 and TT#13, for <1 mm sieve fractions; and HWMK24, for <1mm and <5 μm size fractions. Well-defined bands indicated at 430, 910, 1480, and 1840 nm result from jarosite. The well-defined bands near 1410 nm in the spectra of GCJAR1, TT#12, and TT#35 result from phyllosilicates. Spectra are offset for clarity.

1840 nm. These two features are also reported and discussed by HUNT and ASHLEY (1979) and CLARK *et al.* (1990), who attribute the 1480 nm band to first overtones of OH stretching fundamental vibrations ($2\upsilon_{OH}$). Assignment of the 1840 nm band to $\upsilon_{FeOH} + \upsilon_{OH}$ is consistent with its calculated position (1830 nm) and with assignment of the alunite ($KAl_3(SO_4)_2(OH)_6$) 1770 nm band to $\upsilon_{AlOH} + \upsilon_{OH}$ (HUNT and ASHLEY, 1979). In any event, these two bands are at distinctly different positions than those for common phyllosilicate minerals, including nontronite and montmorillonite (*e.g.,* CLARK *et al.,* 1990). A good example of this difference is the spectrum of GCJAR1 (Fig. 4), which has OH spectral features associated with both jarosite (1480 nm) and phyllosilicate (1410 nm). The spectra of HWMK24, like LNVJAR1, have weak bands near 1480 nm but no detectable feature near 1410 nm, which implies the presence of jarosite and the absence of phyllosilicates.

The reflectivity spectrum of the powder (<90 μm) of tephra particle HWMK24-R3 is relatively featureless and has generally low reflectivity (Fig. 4). This spectrum can be attributed to opaque (titano)magnetites observed in the Mössbauer spectra. The reduced spectral contrast of the absorption bands in HWMK24 (<1 mm) as compared to HWMK24 (<5 μm) likely results from a higher proportion of dark particles (like HWMK24-R3) in the former compared to the latter.

Jarosite formation processes on Mauna Kea

WOLFE *et al.* (1996) report an occurrence of the hyroxysulfate mineral alunite in a sample from another Mauna Kea cinder cone (Puu Poliahu) and attribute its formation to alteration of glass and phenocrysts by hot, sulfur-bearing volcanic gases percolating up through the cone during or soon after its formation. Because its last eruption was ~4 ka before present (WOLFE *et al.,* 1996), there are no volcanic gas measurements available for Mauna Kea. However, volcanic gases from nearby Kilauea Volcano are rich in sulfur. GERLACH (1993) reports that gas compositions from the east rift zone eruption (January, 1983) average 14 and 80 mole % SO_2 and H_2O, respectively. Thus, jarosite formation in HWMK24 likely proceeded by hydrothermal dissolution of silicate glass and minerals by sulfuric acid solutions and subsequent precipitation, under oxidizing conditions, of relatively insoluble jarosite (K-rich). K and Na, whose concentrations are typically ~2 and ~4% as K_2O and Na_2O in hawaiite (*e.g.,* WEST *et al.,* 1988; WOLFE *et al.,* 1996), are derived from the glass and minerals. The formation of jarosite is generally expected at pH <3.5 (VAN BREEMAN, 1982; CARSON *et al.,* 1982; DIXON *et al.,* 1982). This process is similar to sulfuricization as described by CARSON *et al.* (1982) except that the source of sulfur is volcanic gases and not sulfide minerals. Sulfides are not reported in petrographic studies of hawaiitic lavas (*e.g.,* WEST *et al.,* 1988; WOLFE *et al.,* 1996). We know of no other occurrences of jarosite in tephra, and the Mauna Kea occurrence may be the first reported occurrence of jarosite from a sulfur source other than sulfides.

IMPLICATIONS FOR MARTIAN SURFACE MINERALOGY AND PROCESSES

Our results show that jarosite (in addition to nanophase ferric oxide and well-crystalline hematite and titanohematite) occurs as an iron-bearing, oxidative alteration product of Mauna Kea tephra, although it does not appear to be widely distributed. The alteration is pervasive and occurs throughout the volume of porus tephra particles and as a rind on coherent, dense tephra particles. The cubic crystal morphology suggests the jarosite (K-rich) precipitated directly from solution; XRD data show the phase is well-crystalline. The jarosite likely formed as a hydrothermal alteration product of glassy tephra in the cinder cone when hot, sulfur-bearing volcanic gases percolated up through the tephra during or soon after cone formation. What are the implications of these results for Mars?

MURCHIE *et al.* (1993) discuss the ferric mineralogy of Martian bright soils obtained from the ISM near-infrared imaging spectrometer on the Phobos-2 spacecraft. Some of the spectra (*e.g.,* Amazonis Planitia, Pavonis Base, and Juventae Dorsa) have band minima near 850 nm (Fig. 5) and are consistent with a mineral assemblage containing well-crystalline hematite (*e.g.,* MORRIS *et al.,* 1989; BELL *et al.,* 1990; MORRIS and LAUER, 1990; MORRIS *et al.,* 1993). Other spectra (*e.g.,* East and West Oxia and Lunae Planum) have band minima near 910 nm and imply a ferric mineralogy other than hematite. Jarosite is one of the phases suggested by MURCHIE *et al.* (1993) as an explanation for the 910 nm band. As shown in Fig. 5, this suggestion is not inconsistent with the spectrum of HWMK24 (Fig. 5) because the jarosite 910 nm band minimum in HWMK24 corresponds to the feature in East and West Oxia and Lunae Planum.

If the Martian feature at 910 nm results from jarosite, then there are potentially jarosite features at 430, 1480, and 1840 nm. None are apparent in available reflectance spectra of Martian bright

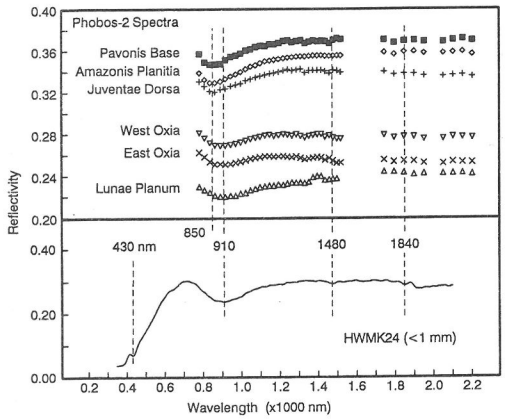

FIG. 5. Comparison of reflectivity spectra for HWMK24 (<1 mm jarositic tephra) and Martian bright regions acquired by the Phobos-2 spacecraft (MURCHIE *et al.*, 1993; MURCHIE, unpublished spectra). Band minima near 850 nm in spectra of Amazonis Planitia, Pavonis Base, and Juventae Dorsa are consistent with the presence of well-crystalline hematite. Band minima near 910 in the spectra of East and West Oxia and Lunae Planum are consistent with the presence of jarosite. The spectrum of HWMK24 results from K-rich jarosite.

regions. This implies (1) that jarosite is not an optically important component in Martian surface materials and some other, presumably ferric, mineralogy is present, or (2) that jarosite is present but these spectral features are not observed for some reason. In the first case, other ferric-mineralogies that have band minima at ~910 nm include ferrihydrite ($\sim Fe_5HO_8 \cdot 4H_2O$), schwertmannite ($\sim Fe_8O_8(OH)_6SO_4$), goethite ($\alpha$-FeOOH), lepidocrocite ($\gamma$-FeOOH), nontronite ($Na_{0.33}Fe_2(Si,Al)_4O_{10} \cdot nH_2O$), and maghemite ($\gamma$-$Fe_2O_3$) (*e.g.*, SHERMAN *et al.*, 1982; SINGER, 1982; MORRIS *et al.*, 1985; MORRIS, unpublished results).

In the second case, the 1480 and 1840 nm jarosite bands might not be apparent in the spectra of East and West Oxia and Lunae Planum because they are too weak to be detected at the spectral resolution and precision of the Phobos-2 data (MURCHIE *et al.*, 1993). That this might be the case is shown by the spectrum of HWMK24 for which the 1480 and 1840 nm features are significantly less intense than the 910 nm feature. The 430 nm jarosite band is more likely to be detected, but the Phobos-2 data do not extend to wavelengths below ~750 nm, and ground-based observations near this wavelength are frequently contaminated by strong solar and stellar emission features (*e.g.*, BELL, 1992). An additional complication is that, even if 430 and 920 nm bands are present in Martian spectral data, assignment to jarosite is equivocal because nontronite (an Fe-smectite) has ferric bands at nearly the same positions (*e.g.*, SINGER, 1982).

In summary, assignment of the Martian 910 nm band to jarosite on the basis of spectral data is equivocal until the presence of bands near 430, 1480, and 1840 nm can be demonstrated. If the results of elemental analyses for Martian soil and SNC meteorites, which indicate low abundances of K (CLARK *et al.*, 1982; MCSWEEN, 1985), are valid for surface regions with the band at 910 nm, hydronium- and/or sodium-rich jarosite ($(H_3O,Na)Fe_3(SO_4)_2(OH)_6$) would be present (BURNS, 1988). Alternatively, the presence of jarosite could imply surface regions of Mars that are rich in K and Na.

If jarosite is present on Mars, what are its formation processes? Burns and coworkers (BURNS, 1988, 1993; BURNS and FISHER, 1990a,b) have suggested that massive and disseminated iron sulfide mineralization occurs near the Martian surface in association with komatiitic volcanism. Jarosite could result from oxidative weathering of the sulfides (pyrrhotite and pentlandite) disseminated in komatiitic basalts (BURNS, 1988, 1993). Oxidative weathering of iron sulfides produced the jarosite in our samples GCJAR1, TT#12, and TT#35 (NORTHROP and WHITNEY, 1987; TOWNSEND, 1987). This study documents an additional formation process for jarosite on Mars which does not involve oxidative alteration of iron sulfides (BURNS, 1987, 1988; BURNS and FISHER, 1990a,b). Namely, acid sulfate weathering of iron-bearing glass and minerals under oxidizing conditions and for which the source of sulfur is volcanic gases and/or fluids.

Acknowledgements—We dedicate this manuscript on rogerburnsite (jarosite) to the late Roger G. Burns who was a strong advocate for its presence on the Martian surface. Roger is greatly missed, both as an exemplary person and as a distinguished scientist. This paper has benefited from discussions with Ed Wolfe, Terry Gerlach, and Del Fanning and the reviews of Scott Murchie and Phil Ihinger. We thank Scott Murchie for revised Phobos-2 IMS spectra. This work was supported by NASA's Planetary Materials and Geochemistry Program.

REFERENCES

ALLEN C. C., GOODING J. L., JERCINOVIC M. and KEIL K. (1981) Altered basaltic glasses: A terrestrial analog to the soil of Mars. *Icarus* **45**, 347–369.

ALLEN C. C., GOODING J. L. and KEIL K. (1982) Hydrothermally altered impact melt rock and breccia: Contributions to the soil of Mars. *J. Geophys. Res.* **87**, 10083–10101.

BELL III J. F. (1992) Charge-coupled device imaging

spectroscopy of Mars. 2. Results and implications for Martian ferric mineralogy. *Icarus* **100,** 575–597.

BELL III J. F., MCCORD T. B. and OWENSBY P. D. (1990) Observational evidence of crystalline iron oxides on Mars. *J. Geophys. Res.* **95,** 14,447–14,461.

BELL III J. F., MORRIS R. V. and ADAMS J. B. (1993) Thermally altered palagonitic tephra: A spectral and process analog to the soil and dust of Mars. *J. Geophys. Res.* **98,** 3373–3385.

BERKLEY J. L. and DRAKE M. J. (1981) Weathering on Mars: Antarctic analogue studies. *Icarus* **45,** 231–249.

BURNS R. G. (1980) Does feroxyhyte occur on the surface of Mars? *Nature* **185,** 647.

BURNS R. G. (1987) Ferric sulfates on Mars. *Proc. Lunar Planet. Sci. Conf. 17th,* E570-E574.

BURNS R. G. (1988) Gossans on Mars. *Proc. Lunar Planet. Sci. Conf. 18th,* 713–721.

BURNS R. G. (1993) Rates and mechanisms of chemical weathering of ferromagnesium silicate minerals on Mars. *Geochim. Cosmochim. Acta* **57,** 4555–4574.

BURNS R. G. and FISHER D. S. (1990a) Iron-sulfur mineralogy of Mars: Magmatic evolution and chemical weathering products. *J. Geophys. Res.* **95,** 14415–14421.

BURNS R. G. and FISHER D. S. (1990b) Evolution of sulfide mineralization on Mars. *J. Geophys. Res.* **95,** 14169–14173.

CARSON C. D., FANNING D. S. and DIXON J. B. (1982) Alfisols and Utisols with acid sulfate weathering features in Texas, p. 127–146. In *Acid Sulfate Weathering* (eds. J. A. KITTRICK et al.), Spec. Pub. 10, SSSA, Madison, WI.

CLARK B. C., BAIRD A. K., WELDON R. J., TSUSAKI D. M., SCHNABEL L. and CANDELARIA M. P. (1982) Chemical composition of martian fines. *J. Geophys. Res.* **87,** 10059–10067.

CLARK R. N., KING T. V. V., KEJWA M. and SWAYZE G. A. (1990) High spectral resolution reflectance spectroscopy of minerals. *J. Geophys. Res.* **95,** 12,653–12,680.

COEY J. M. D., MORUP S., MADSEN M. B. and KNUDSEN J. M. (1990) Titanomaghemite in magnetic soils on Earth and Mars. *J. Geophys. Res.* **95,** 14423–14425.

DIXON J. B., HOSSNER L R., SENKAYI A. L. and EGASHIRA K. (1982) Mineralogical properties of lignite overburden as they relate to mine spoil reclamation, p. 169–191. In *Acid Sulfate Weathering* (eds. J. A. KITTRICK *et al.*), Spec. Pub. 10, SSSA, Madison, WI.

DONER H. E. and LYNN W. C. (1989) Carbonate, halide, sulfate, and sulfide minerals, p. 279–330. In *Minerals in Soil Environments,* 2nd edition, (eds. J. B. DIXON and S. B. WEED) SSSA, Madison, WI.

EVANS D. L. and ADAMS J. B. (1979) Comparison of Viking Lander multispectral images and laboratory reflectance spectra of terrestrial samples. *Proc. Lunar Planet. Sci. Conf. 10th,* 1829–1834.

EVANS D. L. and ADAMS J. B. (1980) Amorphous gels as possible analogs to martian weathering products. *Proc. Lunar Planet. Sci. Conf. 11th,* 757–763.

GERLACH T. M. (1993) Oxygen buffering of Kilauea volcanic gases and the oxygen fugacity of Kilauea basalt. *Geochim. Cosmochim. Acta* **57,** 795–814.

GOLDEN D. C., MORRIS R. V., MING D. W., LAUER JR. H. V. and YANG S. R. (1993) Mineralogy of three slightly palagonitized tephra samples from the summit of Mauna Kea, Hawaii. *J. Geophys. Res.* **98,** 3401–3411.

GOODING J. L. and KEIL (1978) Alteration of glass as a possible source of clay minerals on Mars. *Geophys. Res. Lett.* **5,** 727–730.

HARGRAVES R. B., COLLINSON D. W., ARVIDSON R. V. and SPITZER C. R. (1977) The Viking magnetic properties experiment: Primary mission results. *J. Geophys. Res.* **82,** 4547–4558.

HARGRAVES R. B., COLLINSON D. W., ARVIDSON R. E. and CATES P. M. (1979) Viking magnetic properties experiment: Extended mission results. *J. Geophys. Res.* **84,** 8379–8384.

HUNT G. R., SALISBURY J. W. and LENHOFF C. J. (1971) Visible and near-infrared spectra of minerals and rocks: IV. Sulfides and sulfates. *Modern Geology* **3,** 1–14.

HUNT G. R. and ASHLEY R. P. (1979) Spectra of altered rocks in the visible and near infrared. *Econ. Geol.* **74,** 1613–1629.

MCSWEEN H. Y., Jr. (1985) SNC meteorites: Clues to Martian petrolgic evolution? *Rev. Geophys.* **23,** 391–416.

MCCORD T. B., SINGER R. B., HAWKE B. R., ADAMS J. B., EVANS D. L., HEAD J. W., MOUGINIS-MARK P. J., PIETERS C. M., HUGENIN R. L. and ZISK S. H. (1982) Mars: Definition and characterization of global surface units with emphasis on composition. *J. Geophys. Res.* **87,** 10129–10148.

MORRIS R. V., AGRESTI D. G. LAUER Jr. H. V., NEWCOMB J. A., SHELFER T. D. and MURALI A. V. (1989) Evidence for pigmentary hematite on Mars based on optical, magnetic, and Mössbauer studies of superparamagnetic (nanocrystalline) hematite. *J. Geophys. Res.* **94,** 2760–2778.

MORRIS R. V., GOLDEN D. C., BELL III J. F., LAUER JR. H. V. and ADAMS J. B. (1993) Pigmenting agents in Martian soils: Inferences from spectral, Mössbauer, and magnetic properties of nanophase and other iron oxides in Hawaiian palagonitic soil PN-9. *Geochim. Cosmochim. Acta* **57,** 4597–4609.

MORRIS R. V., GOLDEN D. C., BELL III J. F. and LAUER JR. H. V. (1995) Hematite, pyroxene, and phyllosilicates on Mars: Implications from oxidized impact melt rocks from Manicouagan Crater, Quebec, Canada. *J. Geophys. Res.* **100,** 5319–5328.

MORRIS R. V., GOODING J. L., LAUER JR. H. V. and SINGER R. B. (1990) Origins of Marslike spectral and magnetic properties of a Hawaiian palagonitic soil. *J. Geophys. Res.* **95,** 14427–14434.

MORRIS R. V. and LAUER JR. H. V. (1990) Matrix effects for reflectivity spectra of dispersed nanophase (superparamagnetic) hematite with application to Martian spectral data. *J. Geophys. Res.* **95,** 5101–5109.

MORRIS R. V., LAUER JR. H. V., LAWSON C. A., GIBSON JR. E. K., NACE G. A. and STEWART C. (1985) Spectral and other physicochemical properties of submicron powders of hematite (-Fe_2O_3), maghemite (-Fe_2O_3), magnetite (Fe_3O_4), goethite (-FeOOH), and lepidocrocite (-FeOOH). *J. Geophys. Res.* **90,** 3126–3144.

MOSKOWITZ B. M. and HARGRAVES R. B. (1982) Magnetic changes accompanying the thermal decomposition of nontronite (in air) and its relevance to martian mineralogy. *J. Geophys. Res.* **87,** 10,115–10,128.

MURCHIE S., MUSTARD J., BISHOP J., HEAD J. and PIETERS C. (1993) Spatial variations in the spectral properties of bright regions on Mars. *Icarus* **105,** 454–468.

MUSTARD J. F. and BELL III J. F. (1994) New composite reflectance spectra of Mars from 0.4 to 3.14 m. *Geophys. Res. Lett.* **21,** 3353–3356.

NEWSOM H. E. (1980) Hydrothermal alteration of impact melt sheets with implications for Mars. *Icarus* **44,** 207–216.

NORTHROP H. R. and WHITNEY G. (1987) Clays and associated minerals in the alum mountain fossil geothermal system near Gila Hot Springs, Grant County, New Mexico, p. 1–12. In MUMPTON F. A. (ed.), Zeo-Trip '87, International Committee on Natural Zeolites, Brockport, NY.

POSEY-DOWTY J., MOSKOWITZ B., CRERAR D., HARGRAVES R., TANENBAUM L. and DOWTY E. (1986) Iron oxide and hydroxide precipitation from ferrous solutions and its relevance to martian surface mineralogy. *Icarus* **66,** 105–116.

SHERMAN D. M., BURNS R. G. and BURNS V. M. (1982) Spectral characterization of the iron oxides with application to the martian bright region mineralogy. *J. Geophys. Res.* **87,** 10169–10180.

SHERMAN D. M. and WAITE T. D.(1985) Electronic spectra of Fe^{3+} oxides and oxide hydroxides in the near IR to near UV. *Am. Mineral.* **70,** 1262–1269.

SINGER R. B. (1982) Spectral evidence for the mineralogy of high-albedo soils and dust on Mars. *J. Geophys. Res.* **87,** 10159–10168.

SINGER R. B. (1985) Spectroscopic observation of Mars. *Adv. Space Res.* **5,** 59–68.

SINGER R. B., MCCORD T. B., CLARK R. N., ADAMS J. B. and HUGUENIN R. L. (1979) Mars surface composition from reflectance spectroscopy: A summary. *J. Geophys. Res.* **84,** 8415–8425.

SODERBLOM L. A. and WENNER D. B. (1978) Possible fossil H_2O liquid-ice interfaces in the Martian crust. *Icarus* **34,** 622–637.

STEVENS J. H., POLLAK H., ZHE L., STEVENS V. E., WHITE R. M. and GIBSON J. L. (1983) *Mössbauer Handbook. Mineral: Data Handbook.* Mössbauer Effect Data Center, University of North Carolina, Ashville, NC.

TOWNSEND T. E. (1987) Discrimination of iron alteration minerals in visible and near-infrared reflectance data. *J. Geophys. Res.* **92,** 1441–1454.

VAN BREEMAN N. (1982) Genesis, morphology and classification of acid sulfate soils in coastal plains. p. 95–108. In *Acid Sulfate Weathering,* (eds. J. A. KITTRICK *et al.*) Spec. Pub. 10, SSSA, Madison, WI.

WEST H. B., GARCIA M. O., FREY F. A. and KENNEDY A. (1988) Nature and cause of compositional variation among the alkalic cap lavas of Mauna Kea Volcano, Hawaii. *Contrib. Mineral. Petro.* **100,** 383–397.

WOLFE E. W., WISE W. S. and DALRYMPLE G. B. (1996) *The Geology and Petrology of Mauna Kea Volcano, Hawaii: A Study of Postshield Volcanism,* U. S. Geological Survey Prof. Paper 1557, in press.